

Nonadiabatic wave packet dynamics: Experiment and theory in IBr

Moshe Shapiro

Department of Chemical Physics, The Weizmann Institute of Science, Rehovot, 76100 Israel

Marc J. J. Vrakking

FOM Institute for Atomic & Molecular Physics, Kruislaan 407, 1098 SJ Amsterdam, The Netherlands

Albert Stolow^{a)}

Steeacie Institute for Molecular Sciences, National Research Council of Canada, Ottawa, Ontario K1A 0R6, Canada

(Received 21 August 1998; accepted 27 October 1998)

We present an experimental and a theoretical study of nonadiabatic wave packet dynamics in the intermediate coupling regime as exhibited by the IBr molecule. Using a femtosecond pump–probe molecular beam technique, we generated a wave packet which evolves on the electronically excited $B^3\Pi_0^+/Y(0^+)$ coupled states. The wave packet dynamics was detected by a time-delayed probe pulse which induced two photon ionization to the ground state of the IBr^+ ion. The study consisted of a systematic variation of the pump laser wavelength from the crossing point of the two coupled states to the dissociation limit of the bound diabatic state. The theoretical study is based on the convolution of the products of the energy resolved $X^1\Sigma^+ \rightarrow B^3\Pi_0^+/Y(0^+)$ bound–free dipole matrix elements and the free–bound two-photon ionization amplitudes (calculated exactly using the artificial channel method) with the profiles of the pump and probe pulses. The theoretical calculations reproduce the general decay, recurrence, and revivals observed experimentally. The importance of treating nonadiabatic dynamics beyond the Landau–Zener approximation, as well as the utility of femtosecond pump–probe techniques in probing simultaneously short and long lived resonances is demonstrated. © 1999 American Institute of Physics. [S0021-9606(99)00305-0]

I. INTRODUCTION

The nonadiabatic coupling of electronic and nuclear motions lies at the heart of the photochemistry of polyatomic molecules. These so-called radiationless transitions, such as internal conversion, lead to electronic to vibrational energy transfer and are thus often responsible for the ensuing chemistry. In some cases, even “thermal” chemistry may be profitably thought of from this point of view. The “movement” of an electron from the bond being broken to the bond being formed is induced by a nuclear motion—the collision—and may be thought of as an electronically nonadiabatic process. The transition state potential extremum may in fact originate from an avoided crossing with a higher lying electronic surface. Nonadiabatic processes are the rule rather than the exception in the spectroscopy and photochemistry of excited states of polyatomic molecules and underlie important biochemical mechanisms such as vision and photosynthesis.^{1–4}

The Born–Oppenheimer approximation, an adiabatic separation of electronic from nuclear degrees of freedom, allows us to define one of the most useful concepts in chemistry—the potential energy surface. It allows us to “picture” the trajectories and, hence, reaction paths of the constituent atoms during a chemical process. The breakdown of the approximation due to electron–nuclear coupling leads to the mixing of electronic and nuclear states and the simple concept of a trajectory fails. The multimode dynamics of these systems is inherently complicated and full treatments

of the coupled problem remain quite challenging.^{5,6} Consequently, approaches to dealing with this present situation often rely on reduced dimensionality descriptions of the dynamics in terms of wave packet motion on a limited number of potential energy surfaces. As a first approximation, the nonadiabatic steps are often treated in terms of one-dimensional surface-hopping models using, for example, Landau–Zener theory to calculate the transition probabilities.

Time domain studies of isolated molecules can be complementary to the frequency domain, especially in cases where there are broad ranges of photodissociation resonance linewidths and may often shed new light on the dynamics.^{4,7,8} Wave packet motion in diatomic molecules represents the simplest model system where curve crossing manifests itself and, as such, serves as a basis for understanding limits to the low-dimensionality approximation often used in polyatomic nonadiabatic dynamics. Nonadiabatic wave packet studies in diatomic molecules have been carried out on systems such as NaI, where two diabatic potential energy curves are strongly coupled^{2,9–13} and, in our previous studies, on the IBr molecule.^{14–16} The latter represents the interesting case of intermediate coupling: a complete failure of the Born–Oppenheimer approximation where the wave packet evolution cannot be described by either the diabatic (weak coupling) or adiabatic (strong coupling) approximations.^{17,18} In this article, we present details of a combined experimental–theoretical study of wave packet dynamics in IBr. A numerical wave packet calculation, addressing the same experiments reported here, is presented by Hus-

^{a)}Electronic mail: albert.stolow@nrc.ca

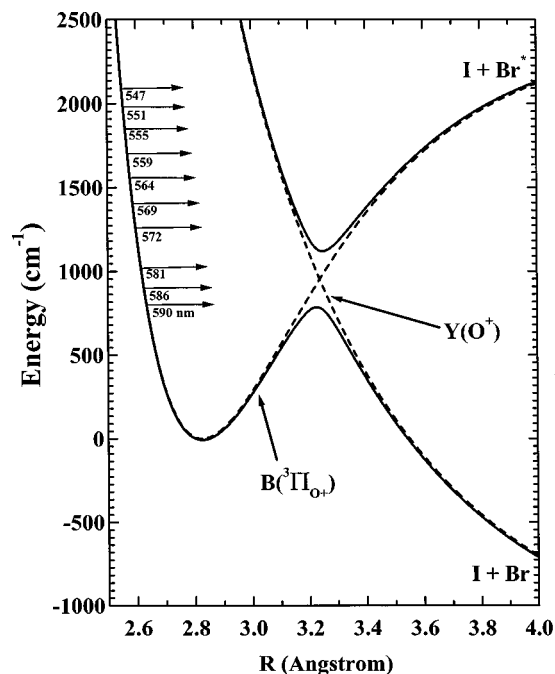
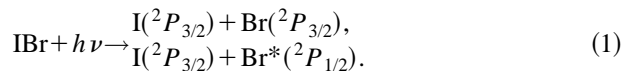


FIG. 1. Intermediate case coupling in IBr. The dashed lines represent the diabatic bound B state, leading to excited state products, and the dissociative Y state, leading to ground state products. The solid lines represent the adiabatic potentials calculated using an R -independent coupling strength of 90 cm^{-1} . For details, see the text. In intermediate case coupling, neither the solid nor the dashed lines fully represent the dynamics. The experiments were performed with ten pump wavelengths ranging from 590 to 547 nm, as shown by the arrows.

sain and Roberts (HR) in the following article.

The low resolution absorption spectrum of IBr¹⁹ has two broad features with maxima at 500 and 270 nm, respectively. The visible band has two open channels:



The main oscillator strength is carried by a bound state (the $B^3\Pi_{0+}$ state) which correlates with $\text{I}(^2P_{3/2}) + \text{Br}^*(^2P_{1/2})$ products. The ground state $\text{I}(^2P_{3/2}) + \text{Br}(^2P_{3/2})$ products are formed by predissociation due to a curve crossing with a repulsive state [the $Y(0^+)$ state]. In the present work, with wavelengths greater than 545 nm, we are concerned only with the predissociation channel to the ground state products.

The $X^1\Sigma^+$ electronic ground state of IBr has the configuration $\sigma^2\pi^4\pi^4\sigma^0$. One excited configuration, $\sigma^2\pi^3\pi^4\sigma^1$, having $^3\Pi_{0+}$ symmetry, is dissociative [the $Y(0^+)$ state] and correlates with ground $\text{I} + \text{Br}(^2P_{3/2})$ channel. Another excited configuration, $\sigma^2\pi^4\pi^3\sigma^1$, also with $^3\Pi_{0+}$ symmetry, is bound (the B state) correlates with the $\text{I} + \text{Br}^*(^2P_{1/2})$ channel. As these states have the same symmetry, they exhibit an avoided crossing. Early photodissociation studies¹⁹ on IBr at visible photon energies above the $\text{I} + \text{Br}^*(^2P_{1/2})$ threshold revealed the curve crossing inherent to the problem.²⁰ Subsequent tunable and ultraviolet (UV) laser studies expanded on these results and added details on the potentials.^{21–24}

In Fig. 1 both diabatic (dashed lines) and adiabatic (solid lines) potential energy curves are shown for the IBr mol-

ecule. The diabatic bound $B^3\Pi_{0+}$ and repulsive $Y(0^+)$ state potential energy curves were obtained using parameters of Guo.¹⁸ The lower adiabatic curve is unbound at energies above the crossing point, whereas the upper adiabatic curve is a bound state which is capable of supporting vibrational levels. We emphasize that due to the intermediate strength of the coupling, neither of the solid (adiabatic) nor dashed (diabatic) curves can be used to completely describe the dynamics. The experiments reported here were carried out at ten excitation energies (ranging from 590 nm near the crossing region to 547 nm near the $\text{I} + \text{Br}^*$ dissociation limit), as indicated in the figures. The nonadiabatic coupling strength used by Child,¹⁷ Shapiro *et al.*,^{15,16} and Guo¹⁸ was $150\text{--}170 \text{ cm}^{-1}$, based upon comparisons with Br/Br^* photodissociation branching ratios at $\lambda < 545 \text{ nm}$ and the available spectroscopic data.

The $B^3\Pi_{0+} \leftarrow X^1\Sigma^+$ absorption spectrum of the IBr molecule contains a large number of diffuse bands and there exist only a limited number of regions where sharp rotational structure (due to high J states) can be observed.^{19,25,26} In seminal studies, Child *et al.*^{17,27,28} gave an interpretation to the spectrum: the large majority of rovibrational states rapidly predissociate via coupling to the repulsive $Y(0^+)$ state, which intersects the $B^3\Pi_{0+}$ state above $v' = 5$. Sharp lines in the absorption spectrum arise from a near resonance between rovibrational levels in the bound diabatic $B^3\Pi_{0+}$ state potential well (Fig. 1; dotted line) and the upper adiabatic potential well (Fig. 1; upper solid line). The onset for rapid predissociation is at the crossing point between the two diabatic curves (adiabatic-like behavior), whereas photodissociation at excitation energies above the dissociation threshold for formation of $\text{I} + \text{Br}^*(^2P_{1/2})$ leads predominantly to the production of $\text{I} + \text{Br}^*(^2P_{1/2})$ rather than $\text{I} + \text{Br}(^2P_{3/2})$ (diabatic-like behavior). This evidence suggested that the dissociation dynamics involves a mixture of the diabatic and adiabatic pictures, i.e., the intermediate case. In support of this, the (few) observed rotational constants are found to be intermediate between those expected based on the energy minima of either the diabatic or adiabatic potential wells. The resonance Raman spectrum of IBr was recorded and theoretically modeled¹⁶ both above and below the B -state dissociation threshold, showing clearly effects due to curve crossing.

In our earlier study of rotationally cold IBr wave packet dynamics¹⁴ we presented results from pump-probe ionization experiments for two pump wavelengths: 569 and 551 nm. The probing of the wave packet motion was achieved via two-photon ionization with mass spectrometric detection. At 569 nm the wave packet decayed within ten vibrational periods. By contrast, at 551 nm, long-time oscillations of the wave packet were observed in complete contradiction of the Landau–Zener picture. These oscillations were attributed to interference between diabatic and adiabatic wave packet evolution and are characteristic of the intermediate coupling regime. These regions of relative stability (i.e., the narrowest resonances) were correctly predicted by a simple weak coupling model (based on the Wentzel–Fermi golden rule).

We note that the dissociation of molecules in strong (nonperturbative) laser fields is also related to the problem of

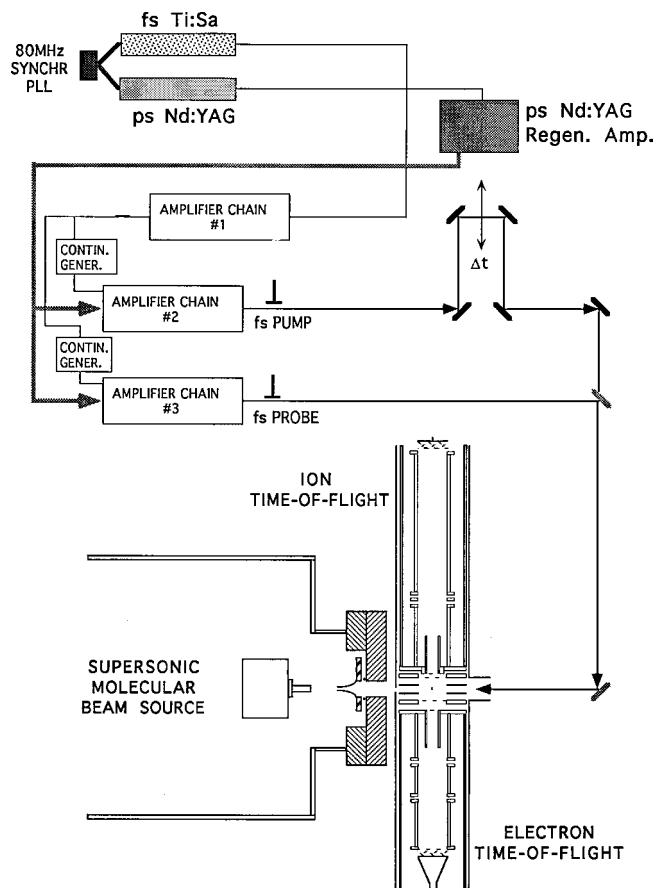


FIG. 2. Experimental setup for pump-probe experiments. A fs Ti:Sa laser is amplified in a dye chain by a high power ps pulse. Continuum is generated and reamplified in two subsequent dye chains, providing the fs pump goes (590–547 nm) and probe (fixed 290 nm) pulses. A pulsed molecular beam into the interaction region of a photoion/photoelectron spectrometer. The total IBr cation signal was collected as a function of the time delay.

interference in nonadiabatic wave packets because laser-induced avoided crossings exhibit many of the same characteristics as the usual avoided crossings.²⁹ In fact, the notion of laser induced molecular stabilization²⁹ is based upon the interference between diabatic and adiabatic wave packet evolution on the dressed potentials, analogous to the phenomenon seen in IBr at specific energies.^{14,15,28}

In the following sections, we discuss the experimental method in more detail and present femtosecond (fs) pump-probe scans as a function of the ten pump laser wavelength. We then go on to discuss the exact fully quantum mechanical formalism used for describing the dynamics and present the detailed simulations of the experimental data.

II. EXPERIMENT

We briefly review the experimental method which is described in detail elsewhere.^{30,31} A schematic view of the experiment is shown in Fig. 2. A fs Ti-sapphire oscillator at 765 nm was amplified in a three-stage prism dye cell amplifier by a synchronized ps Nd:YAG pulse itself amplified in a high power regenerative cavity.³² The amplified Ti:Sa pulse was split and used to generate two white light continua from which the required colors for each of the pump and probe lasers were selected and reamplified in two separate prism

dye chains. The central pump wavelength and bandwidth were variable but the latter was set to yield measured pulse durations of 90 fs. For the probe laser, light around a central wavelength of 580 nm was selected and frequency doubled in a 0.1 mm BBO crystal, giving a 100 fs pulse centered around 290 nm. Note that in our previous communication, this probe laser wavelength was incorrectly reported as 340 nm. The pump and probe lasers were attenuated to approximately 25 and 10 $\mu\text{J}/\text{pulse}$, respectively, and combined using a dichroic beam splitter. The collinear, copropagating lasers were then focused into the molecular beam photoion/photoelectron spectrometer. Care was taken to locate the foci of the visible and UV laser beams away from the molecular beam axis so that neither the visible pump nor the two-photon ultraviolet probe transitions were saturated. Thus, the intensities of the pump and probe lasers were around 10^{10} and 10^{11} W/cm^2 , respectively.

In these experiments, rotationally cold IBr molecules were excited from the ground state ($r_e = 2.47$ Å) to the inner turning point of the diabatic $B^3\Pi_{0+}$ state potential well using the tunable pump pulse. The ensuing wave packet evolution was monitored by measuring the return of the wave packet to the inner turning point of the $B^3\Pi_{0+}$ potential using two-photon ionization with the probe pulse.

IBr⁺ ions ($m/e = 206$, corresponding to $^{127}\text{I}^{79}\text{Br}$) formed by the probe step were collected in the time-of-flight mass spectrometer as a function of the time delay between the pump and probe lasers, which was varied between 0 and 30 ps using a motorized delay stage in the pump laser path. The partial pressure of the IBr sample (Aldrich), which was used without further purification, was controlled to 20 Torr and the IBr was rotationally cooled by seeding in 1 atmosphere of He. We expect that the jet cooled IBr was most likely 5–10 K rotationally and 80–100 K vibrationally. No clusters were observed in the pulsed valve expansion. Care was taken to shield the IBr sample and the gas lines connecting the sample to the molecular beam apparatus from ambient room light and a fresh sample was used on a daily basis.

III. THEORY

The process we wish to explore is the wave packet dynamics resulting from the excitation of the IBr molecule from the $X^1\Sigma^+$ state to the a superposition of continuum states in the $B^3\Pi_{0+}$ and $Y(0^+)$ electronic manifolds. The dissociation due to the excitation pulse [of electric field amplitude $\mathcal{E}_1(t)$] is monitored by a two-photon ionization induced by the probe pulse [of electric field $\mathcal{E}_2(t)$]. One infers the wave packet dynamics in the dissociative states by monitoring the ion concentration as a function of a variable time delay τ between the two pulses. We here assume a combined mass of 207 amu, the average of the two isotopes of IBr (natural abundance: 48% with 206 amu, 52% with 208 amu).

Assuming that both pulses are sufficiently weak, we can write the amplitude for exciting a given continuum state of energy E in the $B^3\Pi_{0+}/Y(0^+)$ excited states by the first pulse at time t as,

$$A(E,t) = \frac{i}{\hbar} \langle \psi^-(E) | \mu_1 | \psi_0 \rangle \int_{-\infty}^t dt' \mathcal{E}_1(t') \exp(i\omega_{E,0}t'), \quad (2)$$

where ψ_0 is the initial bound vibrational state (of energy E_0), $\psi^-(E)$ is an intermediate continuum state (of energy E), μ_1 is the transition-dipole operator between the $X^1\Sigma^+$ ground electronic state and the intermediate $B^3\Pi_{0^+}$ state, and $\omega_{E,0} \equiv (E - E_0)/\hbar$.

With view to the $t \rightarrow \infty$ limit, we write Eq. (2) as

$$A(E,t) = \frac{i}{\hbar} \epsilon_1(\omega_{E,0}) c_E(t) \langle \psi^-(E) | \mu_1 | \psi_0 \rangle, \quad (3)$$

where $\epsilon_1(\omega)$ is the Fourier transform of the first pulse,

$$\epsilon_1(\omega) = \frac{1}{2\pi} \int_{-\infty}^{\infty} dt' \mathcal{E}_1(t') \exp(i\omega t') \quad (4)$$

and $c_E(t)$ are ‘‘preparation’’ coefficients, defined as,

$$c_E(t) = \frac{1}{\epsilon_1(\omega)} \int_{-\infty}^t dt' \mathcal{E}_1(t') \exp(i\omega_{E,0}t'). \quad (5)$$

Clearly, as $t \rightarrow \infty$, $c_E(t) \rightarrow 2\pi$.

For a Gaussian pulse of the form,

$$\mathcal{E}_1(t) = \frac{\mathcal{E}_1^0}{\pi^{1/2}\alpha} \exp[-(t/2\alpha)^2 - i\omega_1 t], \quad (6)$$

for which

$$\epsilon_1(\omega) = \mathcal{E}_1^0 \exp[-\alpha^2(\omega_{E,0} - \omega_1)^2], \quad (7)$$

$c_E(t)$ is given^{23,33} as

$$c_E(t) = \{1 + \text{sgn}(t)(1 - \exp[\beta^2(E,t)]) \times W[\text{sgn}(t)\beta(E,t)]\}, \quad (8)$$

where $\text{sgn}(t) = 1$ for $t \geq 0$, $\text{sgn}(t) = -1$ for $t < 0$. $W[z]$ is the complex error function³⁴ whose argument is given in terms of

$$\beta(E,t) = \alpha(\omega_{E,0} - \omega_1) + it/2\alpha. \quad (9)$$

As a result of the absorption of the first photon, the

$$\Psi(t) = \int dE A(E,t) \psi^-(E) \exp(-iEt/\hbar), \quad (10)$$

wave packet is formed on the coupled $B^3\Pi_{0^+} + Y(0^+)$ excited states.

The pump-probe ionization signal required to make comparisons with the experimental results is calculated as follows. If the center of the second pulse is delayed by time τ relative to the that of the first pulse, the amplitude of observing as $t \rightarrow \infty$ the i th ionic vibrational state, due to the action of the second pulse, is given as,

$$B_i(\tau) = \frac{-4\pi^2}{\hbar^2} \int dE \epsilon_2^2(\omega_{i,E}/2) \langle \psi_i | T_2(\omega_{i,E}/2) | \psi^-(E) \rangle \times A(E,\tau) \exp(-iE\tau/\hbar), \quad (11)$$

where ψ_i are the final bound states of the ion and $T_2(\omega)$ is the two-photon transition operator in second order perturbation theory,

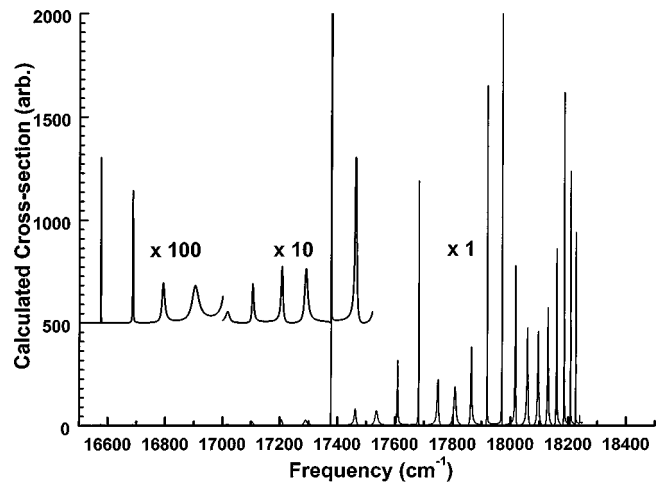


FIG. 3. Calculated absorption spectrum using the ACM method. For a discussion, see the text.

$$T_2(\omega) = \sum_k \frac{\mu_2 |k\rangle \langle k| \mu_2}{\hbar \omega - E_k + E}, \quad (12)$$

and $\omega_{i,E} \equiv (E_i^{\text{ion}} - E)/\hbar$. $P(\tau)$, the probability for producing ions in all states is therefore given, using Eqs. (3) and (11), as,

$$P(\tau) = \sum_i \left| \frac{4\pi^2}{\hbar^2} \int dE c_E(\tau) \epsilon_1(\omega_{E,0}) \epsilon_2^2\left(\frac{\omega_{i,E}}{2}\right) \times \langle \psi_i | T_2\left(\frac{\omega_{i,E}}{2}\right) | \psi^-(E) \rangle \langle \psi^-(E) | \mu_1 | \psi_0 \rangle e^{-iE\tau/\hbar} \right|^2. \quad (13)$$

All the computations reported in this article are based on Eq. (13). The bound-free matrix elements $\langle \psi^-(E) | \mu_1 | \psi_0 \rangle$ and $\langle \psi_i | T_2(\omega_{i,E}/2) | \psi^-(E) \rangle$ were calculated using the artificial channel method (ACM).³⁵ We have used the $X^1\Sigma^+$, the $B^3\Pi_{0^+}$, and $Y(0^+)$ potentials and the coupling between them as parametrized previously,^{15,16} save for the $B^3\Pi_{0^+}/Y(0^+)$ coupling matrix element which was reduced to 90 cm^{-1} , as discussed in detail below.

The theoretical $B^3\Pi_{0^+}/Y(0^+) \leftarrow X^1\Sigma^+$ photodissociation cross section, calculated by the ACM, which is related to the basic bound-free amplitudes of Eq. (2) as,

$$\sigma(E) = \frac{4\pi\omega_{E,0}}{c} |\langle \psi^-(E) | \mu_1 | \psi_0 \rangle|^2, \quad (14)$$

is shown in Fig. 3. It can be seen that there are both broad and narrow resonances as a function of energy in the $16\,500\text{--}18\,400 \text{ cm}^{-1}$ ($606\text{--}543 \text{ nm}$) range. These suggest that there should be regions of relative stability for the diatomic B state.

The free \rightarrow ionic two-photon transitions were also calculated with the ACM, assuming the ionization potential of 9.79 eV derived by Higginson *et al.*³⁶ and the ground IBr^+ Morse potential of Mason *et al.*³⁷

The experimental method is based on two-photon ionization of the coupled $B^3\Pi_{0^+}/Y(0^+)$ states in which intermediate state resonances could potentially play a role. For example, the ion pair E state, could be resonant with the first

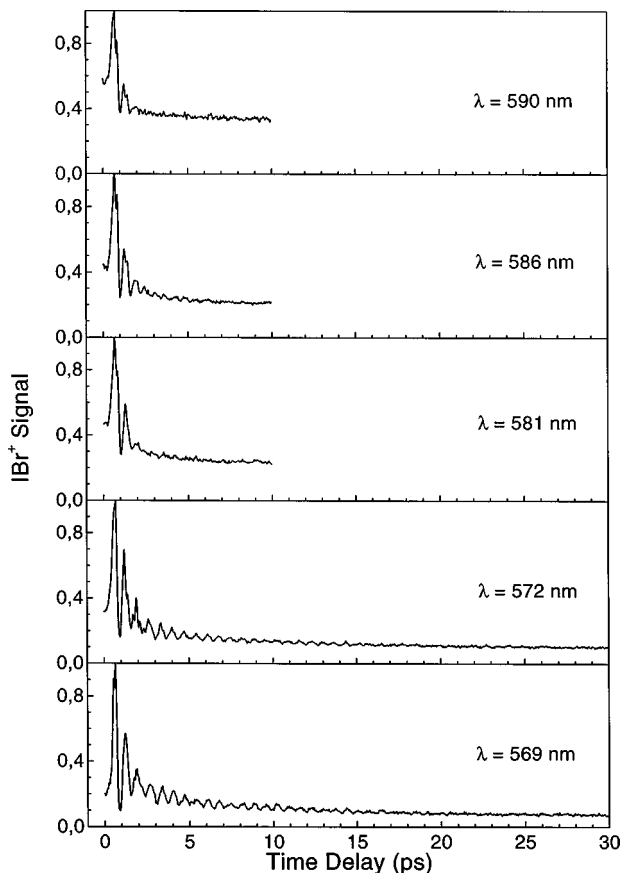


FIG. 4. Pump-probe scans with ion detection ($m/e=206$) for pump wavelengths ranging from 590 to 569 nm. The decay is very rapid (a few vibrations) at longer wavelengths, becoming longer lived at 569 nm.

probe photon. In the article following this one, HR investigated the effects of intermediate resonance by explicitly including wave packet evolution on the intermediate E state during the probe laser pulse. They found that the form of the total IBr^+ ion signal was not significantly affected by inclusion of the E state. Hence our treatment of the two-photon ionization as a nonresonant process is justified.

IV. RESULTS AND DISCUSSION

A. Experimental results

In Figs. 4 and 5, the detected IBr^+ signal is shown as a function of the time delay between the pump and probe lasers for pump central wavelengths in the range of 590–569 and 564–547 nm, respectively. The signals contain a large number of reproducible oscillations and generally show an overall decay, reflecting the predissociation of the excited state. For the wavelengths 590, 586, and 581 nm, the signals show a sharp maximum at zero delay followed by very rapid decay in one or two oscillations (for this reason, these data are shown only over the range of 0–10 ps). At 572 and 569 nm oscillations extending to 10 ps are observed, indicating a decrease in decay rate. At 564 nm, however, fewer oscillations are seen and the decay rate seems to increase again. This illustrates a general observation that the decay rate in fact oscillates as a function of excitation energy.

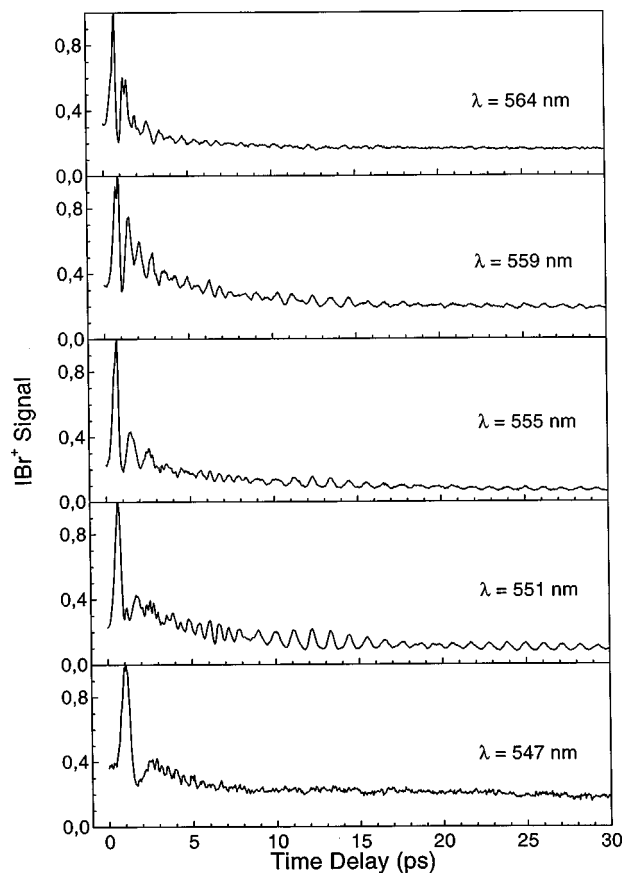


FIG. 5. Pump-probe scans with ion detection ($m/e=206$) for pump wavelengths ranging from 564 to 547 nm. The excited state lifetime is seen to vary strongly with excitation energy. At 551 nm, long oscillations are seen out to beyond 30 ps, in complete violation of the Landau-Zener picture. At 547 nm, the decay is once again very rapid.

Wave packets evolving on single bound anharmonic potentials exhibit oscillation at the classical frequency followed by dephasing and finally revival, as the initial set of phases is eventually reproduced. The revival time is inversely proportional to the product of the anharmonicity and frequency.³⁸ Due to the short lifetimes of the resonances involved, the signal decays on a short time scale compared to the revival time and, hence, no wave packet revivals are seen. For the wavelengths 559, 555, and 551 nm, the decay rates decrease dramatically and oscillations can be seen beyond 30 ps. Furthermore, changing periods of oscillation and revival structure can be seen. For example, at 551 nm, the maximum at zero delay has followed very fast oscillations in the 0–5 ps range. The oscillation period increases in the 5–8 ps range and increases yet again beyond 8 ps. This oscillatory behavior persists on a significantly longer time scale than predicted by simple Landau-Zener calculations (i.e., about 40% of the population dissociates per vibrational period). For a wave packet excited to diabatic B -state vibrational levels in the range $v'=25-30$ (i.e., 551 nm), a revival time of about 25 ps is expected. This can be seen weakly in the 551 nm data of Fig. 5. At the shortest pump wavelength of 547 nm, where part of the wave packet is above the $\text{I}+\text{Br}^*$ dissociation threshold, the signal shows only several very fast oscillations in the 0–5 ps range, essentially disappearing by about 7 ps.

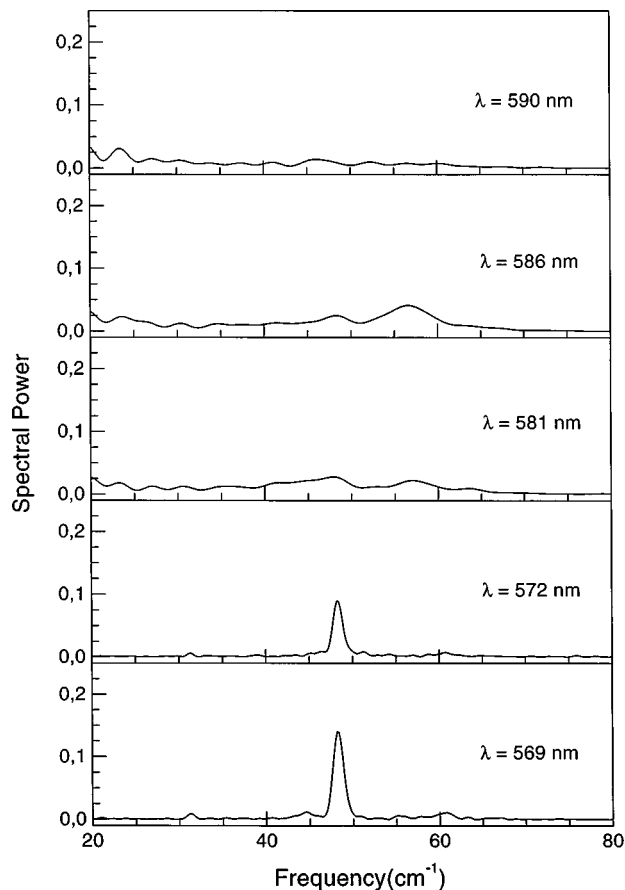


FIG. 6. Fourier transform power spectra of the pump-probe from Fig. 4. When two neighboring resonances are both long lived, they beat against each other to produce a sharp line in the power spectrum. At 572 and 569 nm, two such levels with a frequency spacing around 50 cm^{-1} may be seen.

For the resonances which endure on longer timescales, one expects the Fourier transform (FT) power spectrum to show the presence of sharp frequency components corresponding to energy differences between any two pairs of resonances in the coherent superposition. In these experiments, the bandwidth of the pump laser was sufficient to coherently excite six to eight vibrational levels, depending upon the excitation wavelength. The FTs of the time delay scans of Fig. 4 are shown in Fig. 6, whereas the FTs of the data of Fig. 5 are shown in Fig. 7. Nearest-neighbor coherences at 28.7 , 31.3 , and 33.9 cm^{-1} are observable in scans with pump wavelengths between 551 and 564 nm . By comparison with the data of Eberhard and Sullivan,²⁶ we assign these (using the corrected numbering system of Child) to nearest neighbor coherences $v' = 31 - 30$, $v' = 30 - 29$ and $v' = 29 - 28$, respectively. We note that the assignments used by Selin and by Eberhard and Sullivan has all quanta reduced by three, as compared with Child. The second order (next-nearest neighbor) coherences (e.g., $v' = 31 - 29$) can be seen close to 60 cm^{-1} in the 551 nm FT data. A nearest-neighbor coherence at 48.2 cm^{-1} is observable in scans at pump wavelengths between 559 and 572 nm and corresponds to the vibrational $v' = 23 - 22$, based on recent measurements of the absorption spectrum in a cold molecular beam.³⁹ The FT data show clearly that the resonance lifetimes oscillate as a function of energy.

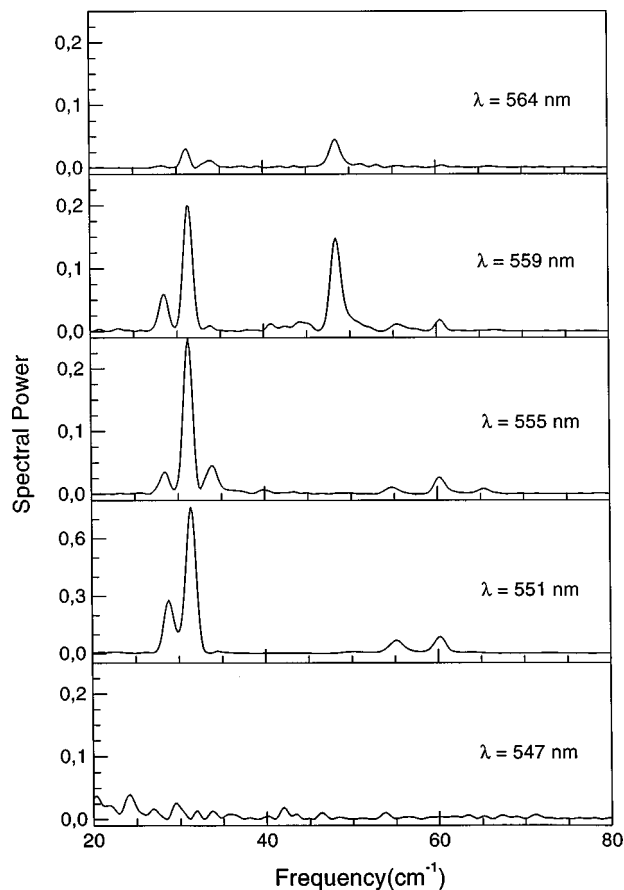


FIG. 7. Fourier transform power spectra of the pump-probe from Fig. 5. At 564 – 551 nm , two groups of narrow resonances may be seen, around 30 and 50 cm^{-1} . A second order coherence (next-nearest neighbors) can also be seen near 60 cm^{-1} . For a discussion, see the text.

The pump laser excites a wave packet which consists of a coherent superposition of resonances with varying widths. At short times (0 – 5 ps) the wave packet consists of a larger number of these and the pump-probe signal rapidly becomes very complicated. At longer times, a significant number of resonances in the coherent superposition have decayed and only a few levels have any significant residual population, resulting in a simplified beat structure, as seen in the 551 nm data of Fig. 5. In the time domain picture, the signal becomes complicated because twice per vibrational period the wave packet moves through the crossing region and splits into two smaller wave packets which can interfere with each other. With reference to Fig. 1, the initial state is a diabatic B -state wave packet which splits into two at the crossing region. A fraction, say 40% , dissociates (adiabatic behavior) to $I + \text{Br}$ products while the rest of the wave packet ‘‘hops’’ (diabatic behavior) to the upper adiabatic curve and continues out to the outer turning point. It subsequently reverses and passes through the crossing point again, splitting a second time. One part continues diabatically by hopping back to the B -state potential. The other part remains for the moment on the upper adiabatic curve. Thus, we have two wave packets, both of which can hop: a diabatic motion following the dashed B -state curve and an adiabatic motion on the upper solid curve in Fig. 1. These two wave packets are strongly coupled by the curve crossing and therefore as they hop they will

interfere with each other. As the classical periods of oscillation will vary with energy for both the diabatic and adiabatic wave packets, we expect this interference to depend strongly on energy. One could imagine, for example, that at characteristic energies the diabatic-adiabatic interference was such that they nearly cancel destructively in the I+Br exit channel. This situation would lead to states which are relatively stable against dissociation. Their continued interference should eventually lead to "standing waves" across both potentials and would in fact represent the narrow scattering resonances involved. Conversely, a narrow scattering resonance can be thought of as originating from an interference between diabatic and adiabatic wave packet evolution.

B. Theoretical results

The calculations presented here used the potential parameters of Levy *et al.*¹⁶ with an R -independent nonadiabatic coupling strength of $V_{12}=90\text{ cm}^{-1}$. The energy resolved $\langle \psi^-(E) | \mu_1 | \psi_0 \rangle$ amplitudes, which generate [according to Eq. (14)] the cross section shown in Fig. 3, were calculated with the ACM. Using these amplitudes, the pump-probe time-resolved spectra were obtained via Eq. (13), basically as a Fourier transform of the convolution of the one- and two-photon bound-free matrix elements and the pump and probe laser pulses. A pump laser bandwidth of 160 cm^{-1} was assumed (i.e., Gaussian transform limit of 90 fs). The ionization probabilities to the separate open ionic vibrational states were then incoherently summed to obtain the integrated ion yield which is directly comparable, with the experimental data.

In Figs. 8 and 9, we show the calculated pump-probe signal (integrated ion yield) for pump laser wavelengths in the ranges 590–569 and 564–547 nm, respectively. At the longest wavelengths, 590 and 581 nm, there are but a few oscillations before the wave packet decays. At the shortest wavelengths, at 547 nm near the I+Br* dissociation limit, the behavior is more complex, but the decay is still fairly rapid. At intermediate energies, the calculations show interference between diabatic and adiabatic evolution which leads to long lifetimes and revival-like features in the pump-probe spectra, seen for example in the 559 and 555 nm plots. Thus, the essential physics of nonadiabatic wave packet dynamics, seen in the experimental results of Figs. 4 and 5, is captured nicely in the theoretical results of Figs. 8 and 9.

There are, however, noticeable deviations between the calculations and the experimental results. At 590 and 586 nm, the calculations reproduce the very fast decay (only 2–3 recurrences are in evidence) quite well. At 581 nm, the experimental results look quite similar to those at 586 nm whereas in the calculations the decay is slower (4 to 5 recurrences are exhibited). At 572 and 569 nm, the calculations reproduce the experiments fairly well, including weak revival structure seen near 6 ps in the 569 nm results. The overall decay at 572 and 569 nm, is, however, faster in the calculations than in the experiments. At 564 nm, the wave packets again decay quickly, although now somewhat faster in the calculations than in experiment.

At 559 and 555 nm, both experiment and theory show the clear effect of diabatic-adiabatic interference, leading to

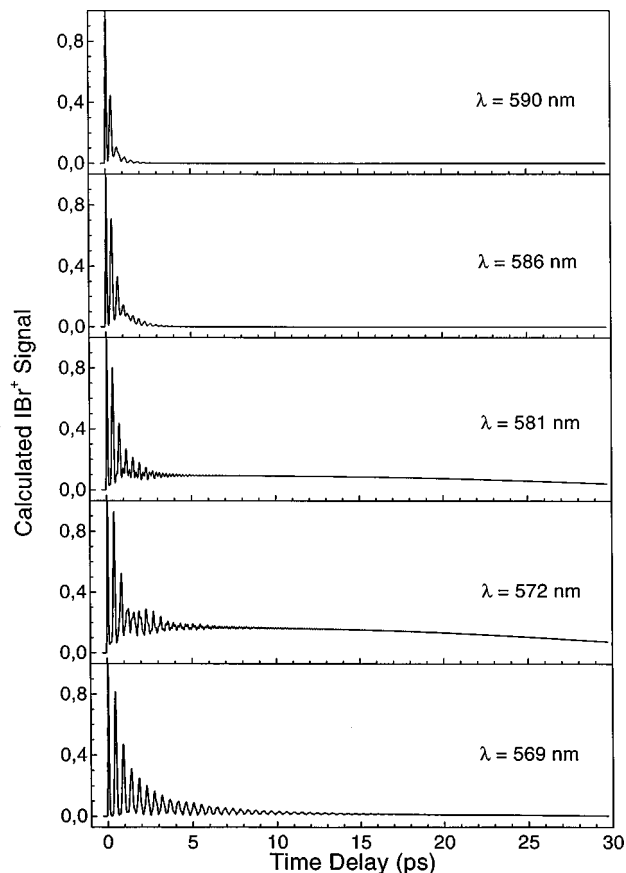


FIG. 8. Calculated pump-probe spectra in the range of 590–569 nm, based on the artificial channel method using the potentials of Fig. 1. The essential physics of the problem, when compared with Fig. 4, is shown in these calculations. The excited state lifetime increases with decreasing wavelength.

long oscillations and revival structures near 13 and 25 ps. In the 555 nm experimental results, a high frequency oscillation is seen near 6 to 7 ps which shows up only weakly and at earlier times (3 to 4 ps) in the calculations. The experimental results at 551 nm show features similar to those at 555 nm, only more clearly and dramatically, indicating strong diabatic-adiabatic wave packet interference. We note that the theory results for 555 nm seem closer to the experimental results at 551 nm. The calculation at 551 nm shows a rapid and complex decay, quite similar in appearance to the experimental results for 547 nm. The theoretical results at 547 nm show broad irregular features not seen in the experiments.

In general, the calculations reproduce the experimental results most quantitatively at low energies near the crossing point. As the energy is increased, experiment and theory show similar features, but: (i) the theoretical plots generally show faster decays than the experimental ones and (ii) the calculations show effects that generally appear at higher energies in the experiment (i.e., the 555 nm theoretical curve looks like the 551 nm experimental one; the 551 nm theoretical curve looks like the 547 nm experimental one).

This detailed comparison of experiment with theory suggests to us that the form of the potentials and, particularly, the coupling strength V_{12} may be in need of some modifica-

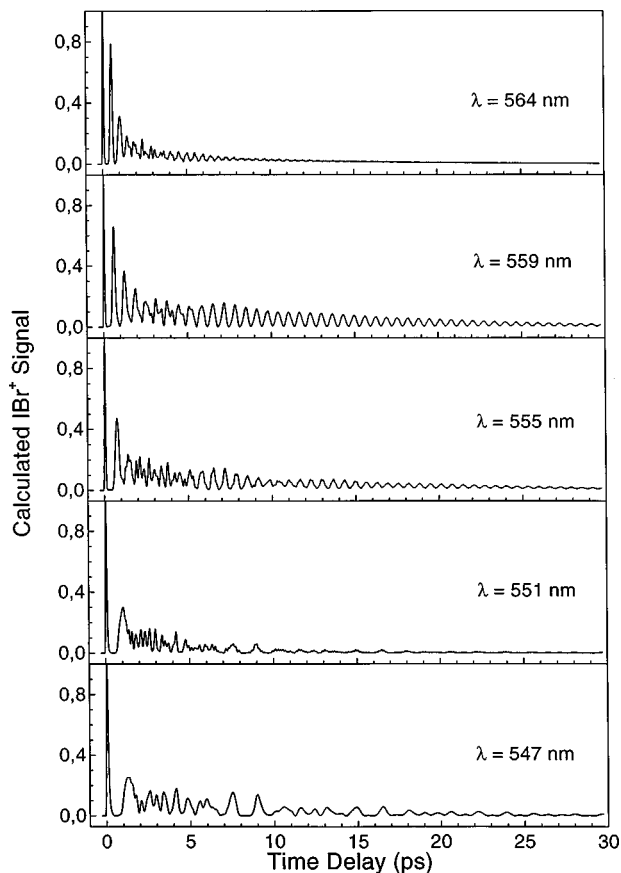


FIG. 9. Calculated pump-probe spectra in the range of 564–547 nm. Again, the essential physics of the problem, when compared with Fig. 5, is shown in these calculations. The excited state lifetime varies strongly with excitation energy.

tion. We began our calculations (not shown here) using an R -independent coupling strength of 170 cm^{-1} , following Child,¹⁷ Shapiro *et al.*,^{15,16} and Guo.¹⁸ We noticed that while this produced some agreement between experiment and theory at the higher energies (555, 551, and 547 nm), it reproduced the experiments rather poorly at energies closer to the crossing region. The choice of Morse parameters for the diabatic B state, the form of the repulsive Y state, and the nonadiabatic coupling strength (which may in general be R dependent) are all relevant to the simulation of the available experimental data. In particular, the potential functions and coupling must be chosen so as to fit the forms of the pump-probe signals and their Fourier transforms (giving directly the level spacings involved) as a function of energy. They are also required to match the frequency domain data of Selin and Volkens *et al.* which are consistent with the time domain data reported here. The development of a new potential is in progress and will be reported elsewhere.³⁹

As a simple first step towards the development of new potentials, we simply varied the coupling strength, keeping all potential parameters unchanged, in order to see if the agreement could be improved. This study suggested that the coupling V_{12} has a value around 90 cm^{-1} near the crossing region, but increases to a value near 170 cm^{-1} near the top of the diabatic B-state potential. We note that this suggestion remains consistent with the observed photochemical Br/Br*

branching ratios used by Child¹⁷ in determining his analysis. In the higher energy regime where both I+Br and I+Br* are open channels, we expect the coupling to be around 170 cm^{-1} . It is only at lower energies, below the I+Br* threshold, that the coupling appears to decrease. If this result is corroborated by the frequency domain studies, it suggests that the assumption of an R -independent coupling may be inappropriate.

We should keep in mind, however, that very quantitative comparisons of these experiments with theory should consider several ancillary problems. The experiments were performed on the molecule $^{127}\text{I}^{79}\text{Br}$ with mass 206 amu whereas the calculations assumed an average mass of 207 amu. The frequency domain results from Volkens *et al.* show in fact that the mass effect on the detailed position of the narrowest resonances is small but not insignificant. Furthermore, the experiments reported here were based upon fs two-photon ionization of the wave packet and therefore the potential effects of intermediate state resonance, autoionization phenomena, and slightly nontransform limited laser pulses on the detailed form of the experimental results might be discerned.

V. CONCLUSION

In this article we have presented results of fs pump-probe experiments on nonadiabatic dynamics in the IBr molecule. The observed wave packet dynamics is complicated as a consequence of the intermediate strength coupling between the diabatic $B^3\Pi_0+$ and $Y(0^+)$ states. In IBr neither a diabatic nor an adiabatic description of the dissociation dynamics is appropriate and, as such, it represents the worst case of the breakdown of the Born-Oppenheimer approximation. Furthermore, the simple Landau-Zener picture of surface hopping is completely invalid in this case. As exemplified by the calculated photodissociation cross sections, the absorption of one photon to the continuum is characterized by the existence of both narrow and broad overlapping resonances. As a result one observes experimentally fast decay processes accompanied by long lived tails. This behavior varies quantitatively as a function of excitation energy. The ability of the pump-probe experiments to monitor both the slow and the fast modes of decay and the recurrence patterns generated by the interference between these diverse resonances provides details of the nonadiabatic dynamics.

The variation of the excited state lifetime with excitation was seen to oscillate as a function of energy. In a time domain picture, the regions of “stabilization” are due to interference between diabatic and adiabatic wave packet evolution. In fact, the existence of narrow resonances at characteristic energies may be generally thought of as arising from an interference between outgoing and incoming flux. We hope that future studies of nonadiabatic dynamics in polyatomic systems will augment the one dimensional results of the present study.

ACKNOWLEDGMENTS

The authors thank Dr. Gareth Roberts and Ahmed Husain (Cambridge) for many helpful discussions and sharing their results during the course of this work. A.S. ac-

knowledges Dr. V. Blanchet, Dr. M. Lezius, and Dr. M. Yu. Ivanov (Steacie Institute) for valuable suggestions. The work of M.J.J.V. is part of the research program of the Stichting voor Fundamenteel Onderzoek der Materie (FOM) which is financially supported by the Nederlandse organisatie voor Wetenschappelijk Onderzoek (NWO). M.S. acknowledges support from Bluma and Bram Appel.

- ¹J. Michl and V. Bonacic-Koutecky, *Electronic Aspects of Organic Photochemistry*, (Wiley, New York, 1990).
- ²M. Shapiro, *J. Phys. Chem.* **97**, 7396 (1993).
- ³R. Schinke, *Photodissociation Dynamics* (Cambridge, Cambridge, England, 1993).
- ⁴V. Blanchet and A. Stolow, *J. Chem. Phys.* **108**, 4371 (1998).
- ⁵G. Stock and W. Domcke, *Adv. Chem. Phys.* **100**, 1 (1997).
- ⁶D. R. Yarkony, *J. Phys. Chem.* **100**, 18612 (1996).
- ⁷A. Zewail, *Femtochemistry: Ultrafast Dynamics of the Chemical Bond* (World Scientific, Singapore, 1994).
- ⁸*Femtosecond Chemistry*, edited by J. Manz and L. Wöste (VCH, Weinheim, Germany, 1995).
- ⁹T. S. Rose, M. J. Rosker, and A. H. Zewail, *J. Chem. Phys.* **88**, 6672 (1988); **91**, 7415 (1989); *Chem. Phys. Lett.* **146**, 175 (1988).
- ¹⁰Ch. Meier, V. Engel, and J. S. Briggs, *J. Chem. Phys.* **95**, 7337 (1991).
- ¹¹P. Cong, A. Mokhtari, and A. H. Zewail, *Chem. Phys. Lett.* **172**, 109 (1990).
- ¹²J. R. Waldeck, M. Shapiro, and R. Bersohn, *J. Chem. Phys.* **99**, 5924 (1993); M. Shapiro, *Faraday Discuss. Chem. Soc.* **91**, 352 (1991).
- ¹³S. Chapman and M. S. Child, *J. Phys. Chem.* **95**, 578 (1991).
- ¹⁴M. J. J. Vrakking, D. M. Villeneuve, and A. Stolow, *J. Chem. Phys.* **105**, 5647 (1996).
- ¹⁵H. Bony, M. Shapiro, and A. Yogeve, *Chem. Phys. Lett.* **107**, 603 (1984).
- ¹⁶I. Levy, M. Shapiro, and A. Yogeve, *J. Chem. Phys.* **96**, 1858 (1992).
- ¹⁷M. S. Child, *Mol. Phys.* **32**, 1495 (1976).
- ¹⁸H. Guo, *J. Chem. Phys.* **99**, 1685 (1993).
- ¹⁹D. J. Seery and D. Britton, *J. Phys. Chem.* **68**, 2263 (1964).
- ²⁰G. E. Busch, R. T. Mahoney, R. I. Morse, and K. R. Wilson, *J. Chem. Phys.* **51**, 837 (1969); J. H. Ling and K. R. Wilson, *J. Chem. Phys.* **65**, 881 (1976).
- ²¹M. S. de Vries, N. J. A. Veen, and A. E. de Vries, *Chem. Phys. Lett.* **56**, 15 (1978).
- ²²M. S. de Vries, N. J. A. Veen, M. Hutchinson, and A. E. de Vries, *Chem. Phys.* **51**, 159 (1980).
- ²³R. J. Donovan and N. Nishi, *Chem. Phys. Lett.* **117**, 286 (1985).
- ²⁴K. W. Jung, J. A. Griffiths, and M. A. El-Sayed, *J. Chem. Phys.* **103**, 6999 (1995).
- ²⁵L.-E. Selin, *Ark. Fys.* **21**, 529 (1962).
- ²⁶W. H. Eberhardt and W. Sullivan, *J. Mol. Spectrosc.* **70**, 270 (1978).
- ²⁷M. S. Child and R. B. Bernstein, *J. Chem. Phys.* **59**, 5916 (1973).
- ²⁸A. D. Bandrauk and M. S. Child, *Mol. Phys.* **19**, 95 (1970).
- ²⁹A. D. Bandrauk, E. Aubenal and J. M. Gauthier, *Laser Phys.* **3**, 381 (1993).
- ³⁰I. Fischer, D. M. Villeneuve, M. J. J. Vrakking, and A. Stolow, *J. Chem. Phys.* **102**, 5566 (1995).
- ³¹I. Fischer, M. J. J. Vrakking, D. M. Villeneuve, and A. Stolow, *Chem. Phys.* **207**, 331 (1996).
- ³²D. M. Villeneuve, I. Fischer, and A. Stolow, *Opt. Commun.* **114**, 141 (1995).
- ³³M. Shapiro, in *Femtosecond Chemistry*, edited by J. Manz and L. Wöste (VCH, Weinheim, Germany, 1995), p. 321.
- ³⁴M. Abramowitz and I. A. Stegun, *Handbook of Mathematical Functions* (Dover, New York, 1965), Eqs. (7.1.3); (7.1.8).
- ³⁵M. Shapiro, *J. Chem. Phys.* **56**, 2582 (1972).
- ³⁶B. R. Higginson, D. R. Lloyd, and P. J. Roberts, *Chem. Phys. Lett.* **19**, 483 (1973).
- ³⁷S. M. Mason and R. P. Tuckett, *Chem. Phys.* **109**, 383 (1986).
- ³⁸M. J. J. Vrakking, D. M. Villeneuve, and A. Stolow, *Phys. Rev. A* **54**, R37 (1996).
- ³⁹E. Volkers, A. Wiskerke, R. Mooiman, M. J. J. Vrakking, and S. Stolte (unpublished).